Journal of Alloys and Compounds 509 (2011) 6824–6828

Contents lists available at ScienceDirect

Journal of Alloys and Compounds

journal homepage: www.elsevier.com/locate/jallcom

Nano-sized Fe-metal catalyst on ZnO–SiO_2: (photo-assisted deposition and impregnation) Synthesis routes and nanostructure characterization

R.M. Mohamed [a,b,*], M.A. Al-Rayyani [a], E.S. Baeissa [a], I.A. Mkhalid [a]

[a] Chemistry Department, Faculty of Science, King Abdel-Aziz University, Jeddah, Saudi Arabia
[b] Advanced Matertials Department, Central Metallurgical R&D Institute, CMRDI, P.O. Box 87 Helwan, Cairo, Egypt

ARTICLE INFO

Article history:
Received 10 January 2011
Received in revised form 15 March 2011
Accepted 16 March 2011
Available online 31 March 2011

Keywords:
Sol–gel technique
Visible photocatalyst
Waste water treatment

ABSTRACT

A nano-sized Fe metal on ZnO–SiO_2 was synthesized using the photo-assisted deposition (PAD) and impregnation routes. The obtained samples were characterized by a series of techniques including X-ray diffraction (XRD), UV–vis diffuse reflectance spectroscopy, N_2 adsorption, extended X-ray absorption fine structure (EXAFS), and transmission electron microscopy (TEM). Photocatalytic reactivity using Fe–ZnO–SiO_2 catalysts under visible-light condition on the degradation of methylene blue dye was evaluated. The results of characterization reveal, a notable photocatalytic activity of PAD:Fe–ZnO–SiO_2 which was about 9 and 12 times higher than that of Img:Fe–ZnO–SiO_2 and ZnO–SiO_2, respectively.

1. Introduction

There has been a lot of attention recently on advanced oxidation processes for water and wastewater decontamination, and heterogeneous photocatalysis is a popular technique in these processes that has been applied to produce reactive species (often the hydroxyl radical) with the purpose of controlling aqueous organic pollutants [1]. One way of generating hydroxyl radicals in aqueous solution is the application of semiconductor photocatalysts which is considered a promising technology in solving environmental pollution problems.

Several semiconductors have band gap energies sufficient for catalyzing a wide range of chemical reactions of environmental interest [2,3]. Among various semiconductors studied, ZnO has been identified as a promising host material and proved to be the most suitable catalyst for widespread environmental applications because of its high photosensitivity, excellent mechanical characteristics, low cost and environmentally safe nature [4,5].

However, a major drawback of ZnO is the large band gap of 3.37 eV, so wavelengths below 400 nm are necessary for excitation. Another disadvantage of ZnO is that charge carrier recombination of photo-generated electron/hole pairs occurs within nanoseconds and the photocatalytic activity is low [4,6–8]. Therefore, it is necessary to improve its visible-light activities by extending its absorption threshold from the UV light region to the visible light region and also reduce the recombination of photo-generated electron/hole. The most promising method to increase the photocatalytic efficiency is the surface modification of ZnO. The surface modification of ZnO can be achieved by metal doping into ZnO. A wide range of metal ions, in particular transition metal ions, have been used as dopants for ZnO because the recombination of photogenerated electrons and holes can be hindered by increasing the charge separation [9–12]. Among various transition metal ions, ferric ion (Fe^{3+}) is considered an interesting doping element due to its half-filled electronic configuration. A proper concentration of Fe^{3+} ions is not only to favor electron–hole separation, but also to narrow its band gap [6]. Also the surface modification of ZnO nanoparticles by preparing charge-transfer catalysts with mixing multi-component oxides can enhance the surface chemical and physical properties and considered as the key for the successful photocatalytic applications of such nanoparticles. Silicon dioxide, SiO_2, has been coupled with semiconductor photocatalyst to enhance the photocatalytic process. SiO_2 has high thermal stability, excellent mechanical strength and helps to create new catalytic active sites due to interaction between semiconductor photocatalyst and SiO_2. Also, at the same time SiO_2 acts as the carrier of semiconductor photocatalyst and helps to obtain a large surface area as well as a suitable porous structure [13–17].

In order to develop the efficient and practical catalysts, a novel strategy is desired to provide nano-sized metal with well-controlled size and dispersability on solid support [18]. Together with such strategy, it is also desired to manipulate the single-site photocatalyst band gap to acquire single-site photocatalyst ability to work under UV and/or visible light radiation. Under UV and/or

* Corresponding author at: Chemistry Department, Faculty of Science, King Abdul Aziz University, P.O. Box 80203 Jeddah: 21589, King Saudi Arbia.
mobile: +966 540715648.
E-mail address: redama123@yahoo.com (R.M. Mohamed).

0925-8388/$ – see front matter © 2011 Elsevier B.V. All rights reserved.
doi:10.1016/j.jallcom.2011.03.098

visible irradiation, these single-site photocatalysts could form a charge transfer excited state which can show the highly active and selective photocatalytic performance [18–20].

In the present work, Fe–ZnO–SiO_2 nanoparticles with large specific surface areas have been synthesized by the application of a photo-assisted deposition (PAD) and impregnation (Img) methods, and the properties of the nanoparticles have been characterized by XRD, TEM, EXAFS, UV–vis/DRS and BET analysis. Furthermore, the photocatalytic reactivity of such nanoparticles has been evaluated using methylene blue dye as a model reaction in the photodegradation process under visible light.

2. Experimental

2.1. Chemicals

Zinc nitrate hexahydrate ($Zn(NO_3)_2{\cdot}6H_2O$), ferric nitrate monohydrate ($Fe(NO_3)_3{\cdot}9H_2O$) and tetraethyl orthosilicate (TEOS) were purchased from Aldrich and selected as the source of zinc and silica, respectively. All chemicals were used in this study used as received without further purification.

2.2. Preparation of ZnO/SiO_2

In a typical procedure, 20 ml TEOS was mixed with ethyl alcohol (C_2H_5OH), ultra pure water (H_2O) and nitric acid (HNO_3) under vigorous stirring for 1 h. The overall molar ratio of TEOS:C_2H_5OH:H_2O:HNO_3 was 1:16:12:0.04. Subsequently, after 60 min, an aqueous solution of $Zn(NO_3)_2{\cdot}6H_2O$ was added in turn into the above solution under vigorous stirring for 30 min. After the above operations, the samples were aged for 24 h. Finally, the obtained samples were evaporated and dried at 80 °C, followed by calcination at 550 °C for 5 h in air.

2.3. Preparation of Fe loaded on ZnO/SiO_2 using PAD method

2 wt% of Fe metal was deposited on ZnO–SiO_2 from aqueous solution of ferric nitrate monohydrate ($Fe(NO_3)_3{\cdot}9H_2O$) under UV-light irradiation. The samples were dried at 100 °C and reduced by H_2 (20 ml/min) at 550 °C for 4 h.

2.4. Preparation of Fe loaded on ZnO/SiO_2 using impregnation method

In a typical impregnation method, the 2 wt% of Fe metal was deposited by a simple impregnation of ZnO–SiO_2 in the absence of light with aqueous solution of ferric nitrate monohydrate. The samples were dried at 100 °C and reduced by H_2 (20 ml/min) at 550 °C for 4 h.

2.5. Characterization techniques

To determine the crystallite sizes and identities of the Fe-loaded on ZnO/SiO_2 nanocomposite photocatalyst, X-ray diffraction (XRD) analysis was carried out at room temperature using Rigaku X-ray diffractometer with Cu Kα radiation over a 2θ collection range of 10–80°. The shape of the samples was tested using Hitachi H-9500 Transmission Electron Microscope (TEM), the prepared samples were prepared by suspending the prepared samples in ethanol, followed by ultrasonication for 30 min, then a small amount of this solution was added onto a carbon coated copper grid and dried before loading the sample in the TEM. Specific surface area was calculated from measurements of N_2-adsorption using Nova 2000 series chromatech apparatus at 77 K. Prior to the measurements all samples were treated under vacuum at 200 °C for 2 h. UV–vis diffuse reflectance spectra (UV–vis–DRS) were recorded in air at room temperature in the wavelength range of 200–800 nm using Shimadzu UV-2450 spectrophotometer. The extended X-ray absorption fine structure (EXAFS) was performed at BL-7C facility [21] of the Photon Factory at the National Laboratory for High Energy Physics, Tsukuba, Tokyo, Japan. A Si (1 1 1) double crystal was used to monochromatize the X-rays from the 2.5 GeV electron storage ring. The K-edge EXAFS spectra of Fe were measured in the fluorescence mode at 25 °C. The Fourier transformed was performed on K^3-weighted EXAFS oscillations in the range of 0–5 Å.

2.6. Photocatalytic activity measurements

A set of photocatalytic degradation of methylene blue (50 ppm) was carried out by cylindrical Pyrex glass photoreactor under visible light irradiation. A 150 W high-pressure mercury lamp was used as the light source (any irradiation below 400 nm removed using cut off filter). The catalysts and solution were separated by filtration; the collected samples were analyzed by UV–vis spectrophotometer (Shimadzu UV-2450). The photodegradation efficiency of methylene blue was calculated applying the following equation:

$$\%\,\text{Photodegradation efficiency} = \frac{C_o - C}{C_o} \times 100$$

where C_o is the original methylene blue content; C is the retained methylene blue in solution.

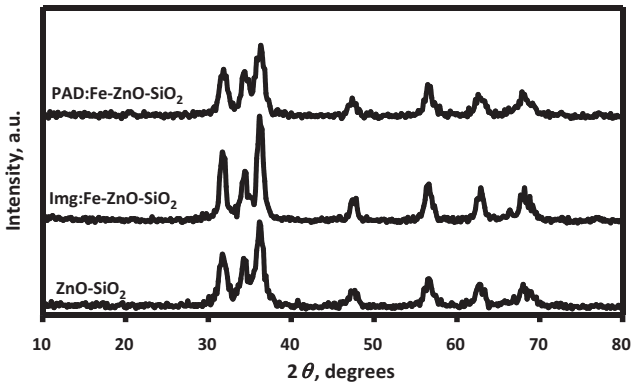

Fig. 1. XRD patterns of the (ZnO–SiO_2, Img:Fe–ZnO–SiO_2 and PAD:Fe–ZnO–SiO_2).

3. Results and discussion

3.1. Phase analysis

The XRD patterns of the ZnO–SiO_2 and Fe-doped ZnO–SiO_2 nanoparticles prepared by (Img) and (PAD) routes are shown in Fig. 1. It can be seen that the diffraction patterns of ZnO–SiO_2 sample and all Fe-doped ZnO–SiO_2, are mainly composed of ZnO phase which still exists after applying both mentioned preparation methods. While, in the Fe-doped samples; no diffraction peaks of Fe were observed, this is probably attributed to the low Fe doping content (ca. 2 wt%). Moreover, it is obvious that, Fe is well dispersed within the ZnO–SiO_2 phase.

3.2. Nanostructure characterization

Fig. 2 displays the Fourier transforms of Pt L_{III}-edge EXAFS spectra of the Fe-loaded catalysts. It can be noticed that, the presence of the peak assigned to the Fe–Fe bond of Fe metal at around 2.5 Å is an indication of the formation of nano-sized Fe metal [22]. In addition, the intensity of the Fe–Fe peak of the PAD:Fe–ZnO–SiO_2 catalyst is smaller than that prepared by impregnation route. These obtained results reveal that the size of Fe metal particles depends on the route of preparation. Fe metal particles formed on (PAD:Fe–ZnO–SiO_2) show smaller particle size than (Img:Fe–ZnO–SiO_2).

The grain size of PAD:Fe–ZnO–SiO_2 and Img:Fe–ZnO–SiO_2 nanocomposite photocatalysts are displayed in TEM images as shown in Fig. 3.

The particle size distribution obtained from the analysis of TEM images is shown in Fig. 4. The results reveal that the nano-sized Fe metal with a mean diameter (d) of ca. 30 nm having a nar-

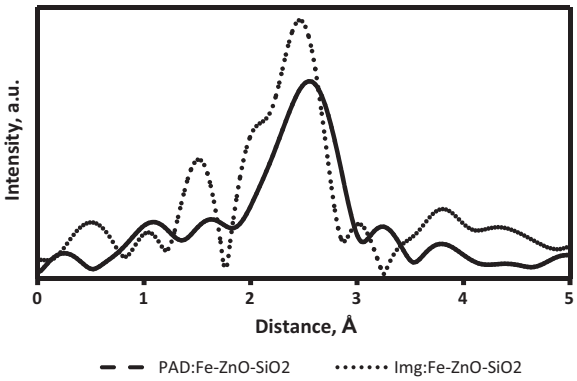

Fig. 2. Fourier transforms of the Pt L_{III}-edge EXAFS spectra for Img:Fe–ZnO–SiO_2 and PAD:Fe–ZnO–SiO_2.

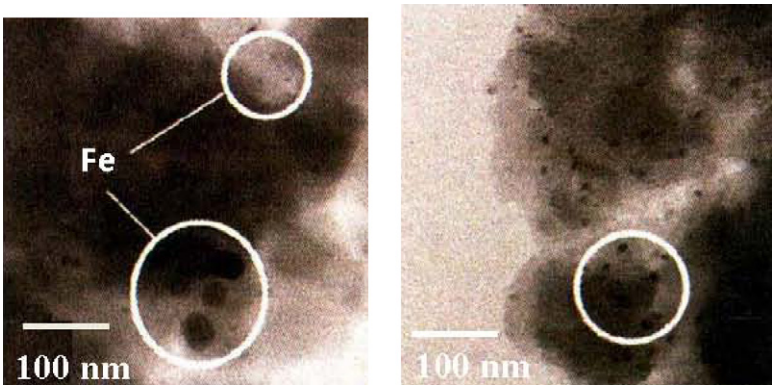

Fig. 3. The TEM images of the Img:Fe–ZnO–SiO_2 (left) and PAD:Fe–ZnO–SiO_2 (right) catalysts after H_2 treatment at 550 °C.

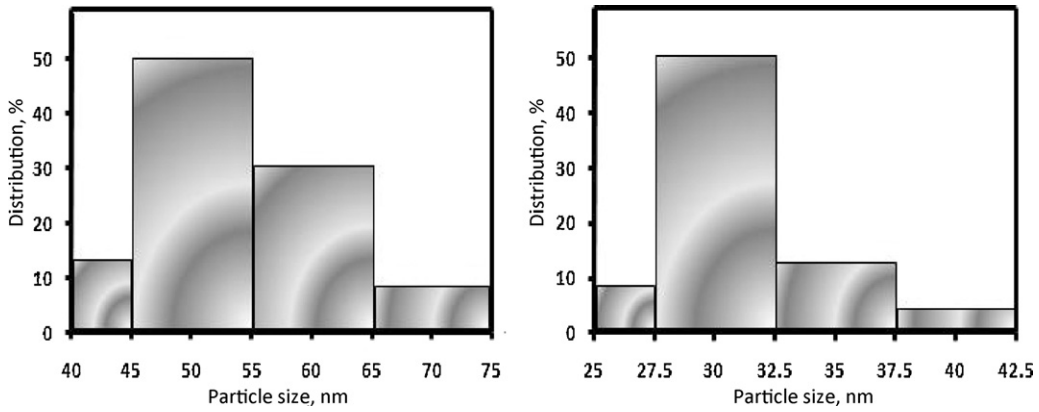

Fig. 4. Size distribution diagrams of Fe metal obtained from the TEM images of the Img:Fe–ZnO–SiO_2 (left) and PAD:Fe–ZnO–SiO_2 (right) catalysts after H_2 treatment at 550 °C.

row size distribution is found on the PAD:Fe–ZnO–SiO_2 catalyst, whereas the aggregated Fe metal within various sizes is observed on Img:Fe–ZnO–SiO_2 catalyst (d = 50 nm) which is in agreement with the results of EXAFS measurement.

3.3. Surface area analysis

The (ZnO/SiO_2, PAD:Fe–ZnO–SiO_2 and Img:Fe–ZnO–SiO_2) powers are characterized by specific surface area S_{BET}. The S_{BET} is 500 m^2/g pertaining to (parent ZnO–SiO_2), otherwise 600 and 700 m^2/g in case of (Img:Fe–ZnO–SiO_2 and PAD:Fe–ZnO–SiO_2) respectively which means about 8.2% and 30.4% increase, respectively S_{BET} value compared to the parent ZnO–SiO_2.

The parameters of surface area and the data calculated from the *t*-plot are collected in Table 1. The obtained results from the N_2-adsorption isotherms for the parent and Fe–ZnO–SiO_2 powders indicate that both are typical of mesoporous solids type IV (not shown here). However, an increase in the adsorption capacity of the ZnO–SiO_2 was observed after introducing Fe ions.

Furthermore, the total pore volume of Fe–ZnO–SiO_2 is higher than that of ZnO–SiO_2. The values of S_{BET} and S_t are generally close in most samples indicating the presence of mesopores. The values of S_{meso} are high compared to that of S_{micro} implying that the main surface is mesoporous solid as represented by the isotherm. The surface texture data are correlated with the catalytic activity as will be mentioned later on.

3.4. UV–vis–DRS analysis

The band-gap value usually reported for pure ZnO phase is 3.37 [8]. However, this value is influenced by the synthesis method, and it is also affected by the existence of impurities doping the crystalline network and also the average crystal size of the semiconductor. In a previous study, different methods for calculating the E_g from the UV–vis reflectance spectra were used. For example, some authors calculated the E_g values by a direct extrapolation of the $F(R)$ spectrum whereas others reported the wavelength corresponding to the maximum absorption [23]. As a consequence, quite different E_g values for ZnO samples are found in the literature. For instance, a threshold wavelength values of 240 nm [24], 290 nm [25], and 360 nm [26] are found corresponding to band gaps 5.15, 4.28, and 3.45, respectively.

Fig. 5 gives UV–vis–DRS of (ZnO–SiO_2, Img:Fe–ZnO–SiO_2 and PAD:Fe–ZnO–SiO_2). The results show that an increase in

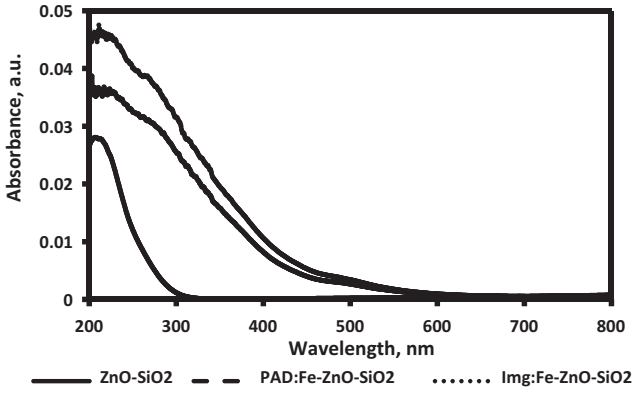

Fig. 5. Diffuse reflectance UV–vis absorption spectra of ZnO–SiO_2, Img:Fe–ZnO–SiO_2 and PAD:Fe–ZnO–SiO_2.

Table 1
Texture parameters of $ZnO–SiO_2$, Img:Fe–$ZnO–SiO_2$ and PAD:Fe–$ZnO–SiO_2$.

Sample	S_{BET} (m^2/g)	S_t (m^2/g)	S_{micro} (cm^2/g)	S_{meso} (cm^2/g)	S_{ext} (cm^2/g)	V_p (cm^3/g)	V_{micro} (cm^3/g)	V_{meso} (cm^3/g)	r (Å)
$ZnO–SiO_2$	500	515	420	208	430	0.588	0.088	0.500	36.00
Img:Fe–$ZnO–SiO_2$	610	618	520	215	530	0.611	0.011	0.600	35.00
PAD:Fe–$ZnO–SiO_2$	700	710	670	230	680	0.788	0.055	0.615	30.00

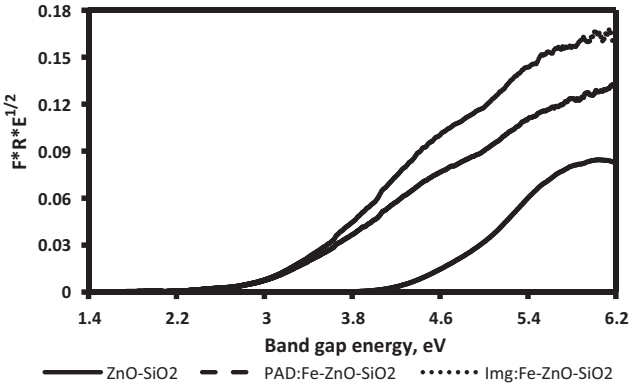

Fig. 6. Band gap calculated from the DR–UV–vis spectra of $ZnO–SiO_2$, Img:Fe–$ZnO–SiO_2$ and PAD:Fe–$ZnO–SiO_2$.

Table 2
The calculated band gap energy of $ZnO–SiO_2$, Img:Fe–$ZnO–SiO_2$ and PAD:Fe–$ZnO–SiO_2$.

Sample	Band gap energy (eV)
$ZnO–SiO_2$	3.2
Img:Fe–$ZnO–SiO_2$	2.9
PAD:Fe–$ZnO–SiO_2$	2.7

absorbency in the visible light region with the iron doping. Therefore, the study of UV–vis radiation absorption is an important tool for the evaluation of the changes in the produced semiconductor materials by different treatments. The value of E_g, the band gap of the semiconductor, can be derived from the spectra by plotting $(F(R)\cdot h\upsilon)^{1/2}$ against $h\upsilon$ as shown in Fig. 6 [27,28] and tabulated as shown in Table 2. The results reveal that the values of calculated band gap for ($ZnO–SiO_2$, Img:Fe–$ZnO–SiO_2$ and PAD:Fe–$ZnO–SiO_2$) are 3.2, 2.9 and 2.7 eV, respectively.

3.5. Evaluation of photocatalytic activity

In order to explore the photocatalytic activity of the prepared nanoparticles in degradation of methylene blue under visible light ($\lambda < 400$ nm). Fig. 7 displays the photocatalytic degradation of methylene blue (using 50 ppm, 300 ml) pertaining to ($ZnO–SiO_2$, Img:Fe–$ZnO–SiO_2$ and PAD:Fe–$ZnO–SiO_2$).

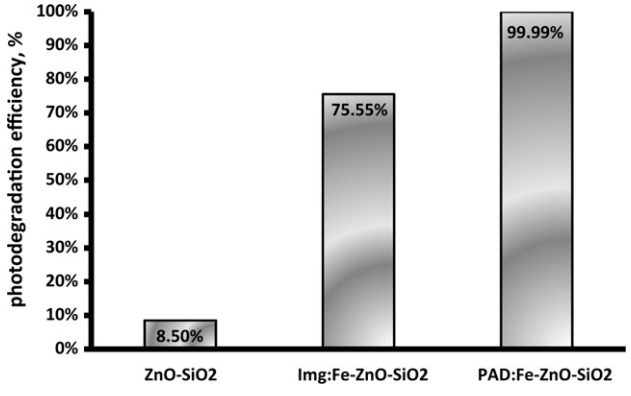

Fig. 7. Photocatalytic degradation of methylene blue (%) for $ZnO–SiO_2$, Img:Fe–$ZnO–SiO_2$ and PAD:Fe–$ZnO–SiO_2$.

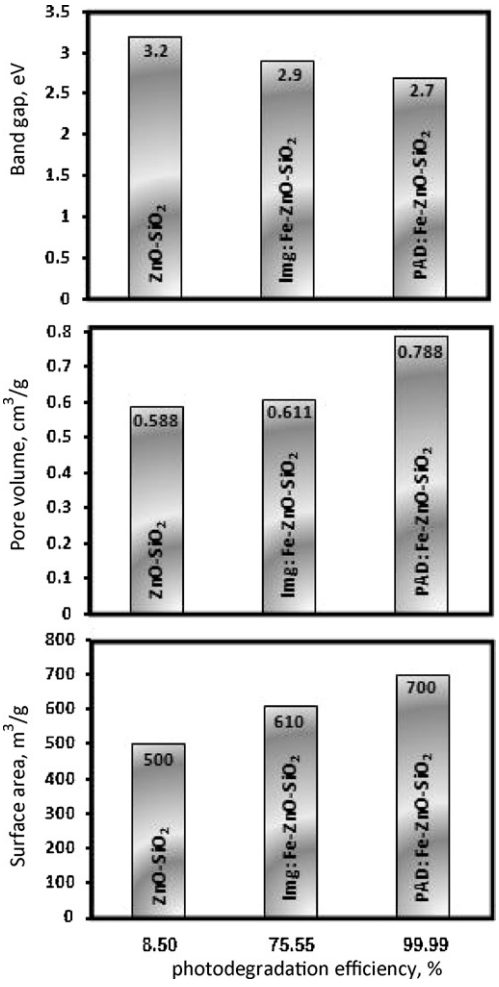

Fig. 8. Effect of physical parameters of the materials on their photocatalytic activity.

The data demonstrate that the photocatalytic activities of the PAD:Fe–$ZnO–SiO_2$ are higher than that of Img:Fe–$ZnO–SiO_2$ and parent $ZnO–SiO_2$. Considering that, the pure Fe oxides do not have photocatalytic oxidation properties, such change may be explained in terms of the differences in interaction between Fe and $ZnO–SiO_2$ that led to several modifications in physical properties such as band gap, particle size and surface texture. Also, one could observe that, the catalytic activity of $ZnO–SiO_2$ generally increased with the addition of Fe promoters. A maximum activity was obtained in case of PAD:Fe–$ZnO–SiO_2$.

The correlation between the photoactivity and the physical properties such as band gap, surface area and pore volume is depicted in Fig. 8. It is obvious that, the photocatalytic activity was at a maximum in the case of PAD:Fe–$ZnO–SiO_2$ in which the surface area and pore volume were maximum but band gap was minimum. In addition, Fig. 8 shows the good correlation between the band gap, surface area and pore volume with the catalytic activity where the

activity is gradually increasing with the decrease of band gap and the increase of the surface area and pore volume.

It is believed that the lack of electron scavengers (surface Zn^{2+}) and hole traps (surface hydroxyl groups) is responsible for the rapid recombination rate of e^-/h^+, which leads to lower photocatalytic activity. The results show that the photocatalytic activities of the Fe-doped ZnO–SiO_2 nanoparticles increased with decreasing the band gap. This is due to the low energy to excite electron from valance band to conduction band. Also, the PAD:Fe–ZnO–SiO_2 has the best photoactivity, since it has the lowest band gap and particle size and the highest surface area and pore volume.

4. Summary

It is obvious that the different preparation routes may affect on physical properties of the catalyst and this appears in different characteristic techniques as shown in the following remarks:

(1) The nano-sized Fe metal with a mean diameter (d) of ca. 30 nm having a narrow size distribution was found on the PAD:Fe–ZnO–SiO_2 catalyst, whereas the aggregated Fe metal with various sizes were observed on Img:Fe–ZnO–SiO_2 catalyst (d = 50 nm).
(2) The calculated values of band gap for ZnO–SiO_2, PAD:Fe–ZnO–SiO_2 and Img:Fe–ZnO–SiO_2 are 3.2, 2.9 and 2.7, respectively.
(3) The N_2-adsorption isotherms for the parent and the Fe–ZnO–SiO_2 are typical of mesoporous solids, the surface area changed from 500 to 610 and 700 m^2/g in case of Img:Fe–ZnO–SiO_2 and PAD:Fe–ZnO–SiO_2, respectively.
(4) The intensity of the Fe–Fe peak of the PAD:Fe–ZnO–SiO_2 catalyst is smaller than the Img:Fe–ZnO–SiO_2 catalyst. These findings suggest that the size of Fe metal particles depends on the preparation method. Fe metal particles formed on the photo-deposited catalyst (PAD:Fe–ZnO–SiO_2) show smaller particle sizes than those obtained from the impregnated catalyst (Img:Fe–ZnO–SiO_2).
(5) Finally TEM micrographs showed the homogenous distribution of Fe over ZnO–SiO_2 matrix which were prepared by PAD method.

References

[1] C. Minero, M. Lucchiari, D. Vione, V. Maurino, Environ. Sci. Technol. 39 (2005) 8936.
[2] L. Deng, S. Wang, D. Liu, B. Zhu, W. Huang, S. Wu, S. Zhang, Catal. Lett. 129 (2009) 513.
[3] S. Qourzal, N. Barka, M. Tamimi, A. Assabbane, A. Nounah, A. Ihlal, Y. Ait-Ichou, Mater. Sci. Eng. C 29 (2009) 1616.
[4] A. Singhal, S. Achary, A. Tyagi, P. Manna, S. Yusuf, Mater. Sci. Eng. B 153 (2008) 47.
[5] W. Shen, Z. Li, H. Wang, Y. Liu, Q. Guo, Y. Zhang, J. Hazard. Mater. 152 (2008) 172.
[6] M. Zhou, J. Yu, B. Cheng, J. Hazard. Mater. B 137 (2006) 1838.
[7] C. Estrellan, C. Salim, H. Hinode, React. Kinet. Catal. Lett. 98 (2009) 187.
[8] C. Klingshirn, Chem. Phys. Chem. 8 (2007) 782.
[9] M. Height, S. Pratsinis, O. Mekasuwandumrong, P. Praserthdam, Appl. Catal. B: Environ. 63 (2006) 305.
[10] T. Han, C. Wu, C. Hsieh, J. Vac. Sci. Technol. B 25 (2007) 430.
[11] R. Ullah, J. Dutta, J. Hazard. Mater. 156 (2008) 194.
[12] R. Slama, F. Ghribi, A. Houas, C. Barthou, L. El Mir, Int. J. Nanoelectro. Mater. 3 (2010) 133.
[13] R. Abd Aziz, I. Sopyan, Indian J. Chem. 48 (2009) 951.
[14] A Anderson, A. Bard, Phys. J. Chem. 99 (1995) 9882.
[15] S. Ruetten, J. Thomas, Photochem. Photobiol. Sci 2 (2003) 1018.
[16] H. Chun, Y. Wang, H. Tang, Appl. Catal. B: Environ. 30 (2001) 277.
[17] D. Comedi, M. Tirado, C. Zapata, S.P. Heluani, M. Villafuerte, P.K. Mohseni, R.R. LaPierr, J. Alloys Compd. 495 (2010) 439.
[18] R.M. Mohamed, I.A. Mkhalid, J. Alloys Compd. 501 (2010) 301.
[19] R.M. Mohamed, I.A. Mkhalid, J. Alloys Compd. 501 (2010) 143.
[20] R.M. Mohamed, J. Mater. Processing Technol. 209 (2009) 577.
[21] N. Masaharu, K. Atsushi, J. Synchrotron Radiat. 6 (1999) 182.
[22] J. Hwang, C. Krebs, B. Huynh, D. Edmondson, E. Theil, J. Penner-Hahn, Science 287 (2000) 122.
[23] R. Davis, Z. Liu, Chem. Mater. 9 (1997) 2311.
[24] H. Yoshida, T. Shimizu, C. Murata, T. Hattori, J. Catal. 220 (2003) 226.
[25] C. Bouvy, B. Su, J. Mater. Sci. Technol. 24 (2008) 495.
[26] G. Mihai, V. Meynen, M. Mertens, N. Bilba, P. Cool, E. Vansant, J. Mater. Sci. 45 (2010) 5786.
[27] M. Anpo, M. Che, Adv. Catal. 44 (1999) 119.
[28] G. Lassaleta, A. Fernaandez, J. Espinoos, A. Gonzaolez-Elipe, J. Phys. Chem. 99 (1995) 1848.